Structure
Article

Quasi-Atomic Model of Bacteriophage T7 Procapsid Shell: Insights into the Structure and Evolution of a Basic Fold

Xabier Agirrezabala,[1,3] Javier A. Velázquez-Muriel,[1,4] Paulino Gómez-Puertas,[2] Sjors H.W. Scheres,[1] José M. Carazo,[1] and José L. Carrascosa[1,*]
[1] Department of Structure of Macromolecules, Centro Nacional de Biotecnología, CSIC, C/Darwin 3, Cantoblanco, 28049 Madrid, Spain
[2] Centro de Biología Molecular Severo Ochoa, CSIC-UAM, C/Francisco Tomás y Valiente, 7 Campus de la Universidad Autónoma de Madrid, Cantoblanco, 28049 Madrid, Spain
[3] Present address: Wadsworth Center, Empire State Plaza, Albany, NY 12201, USA.
[4] Present address: California Institute for Quantitative Biomedical Research, 1700 4th Street, Suite 501, University of California, San Francisco, San Francisco, CA 94158, USA.
*Correspondence: jlcarras@cnb.uam.es
DOI 10.1016/j.str.2007.03.004

SUMMARY

The existence of similar folds among major structural subunits of viral capsids has shown unexpected evolutionary relationships suggesting common origins irrespective of the capsids' host life domain. Tailed bacteriophages are emerging as one such family, and we have studied the possible existence of the HK97-like fold in bacteriophage T7. The procapsid structure at ~10 Å resolution was used to obtain a quasi-atomic model by fitting a homology model of the T7 capsid protein gp10 that was based on the atomic structure of the HK97 capsid protein. A number of fold similarities, such as the fitting of domains A and P into the L-shaped procapsid subunit, are evident between both viral systems. A different feature is related to the presence of the amino-terminal domain of gp10 found at the inner surface of the capsid that might play an important role in the interaction of capsid and scaffolding proteins.

INTRODUCTION

Due to the availability of a great amount of genetic and biochemical information, bacteriophages are good model systems for the experimental analysis of macromolecular assembly. In this context, *E. coli*-infecting phage T7 has been widely used for the study of the morphogenetic pathway of double-stranded DNA phages. Bacteriophage T7 belongs to the Podoviridae family and is the genus representative enclosing the related variant previously known as phage T3. It contains a 40 kb dsDNA genome (Dunn and Studier, 1983) that codes for the structural proteins present in the initial self-assembled precursor: the capsid proteins gp10A and gp10B (obtained from a 10% read-through of the same gene 10 that codes for gp10A [Condron et al., 1991]), the scaffolding gp9, the connector gp8, and the proteins gp14, gp15, and gp16 that built the T7 family-related specific internal core (Serwer, 1976). The assembly of this precursor and its sequential maturation are multistep processes. Once the initial procapsid is generated, the major terminase subunit, gp19, possibly arranged as a hexameric ring (Morita et al., 1995), interacts with the pentameric vertex cavity (Agirrezabala et al., 2005). Then, this prohead-terminase 50S complex interacts with the DNA that forms a complex with the minor subunit, gp18, and the unit length genome is encapsidated through the connector channel (Valpuesta and Carrascosa, 1994; Simpson et al., 2000; Guasch et al., 2002). This DNA translocation is the only viral morphogenetic process driven by ATP hydrolysis (for a review of DNA packaging, see [Fujisawa and Morita, 1997]). During maturation, the scaffolding lattice formed by gp9 is disassembled, and the prohead expands irreversibly into a larger shell. Finally, the tail components (gp11, gp12, and gp17) are sequentially attached (Matsuo-Kato et al., 1981; Steven et al., 1988). The final outcome of this maturation process progresses from the viral precursor (the procapsid) to the final fully infective virion.

The use of cryo-electron microscopy has revealed different viral stages of the morphogenetic pathway (Cerritelli et al., 2003; Agirrezabala et al., 2005). Although the low resolution of these studies does not allow for the molecular details of the different transitions in the maturation of T7 to be drawn, a number of relevant features have been described: the thick procapsid shell (~50 Å) is transformed into a much thinner shell (25 Å), which is accomplished by a significant rearrangement of the major shell subunit interactions. The skew arrangement of the procapsid hexamers (common to other viruses as P22, lambda, HK97, or HSV) is transformed into an almost hexagonal array, while the intercapsomeric distance changes from 110 to 140 Å. Also, the interior of the virion suffers drastic rearrangements: the scaffold is released while the DNA is packaged,

and the core moves along the five-fold axis of the particle and inserts into the shell, allowing its interaction with the tail components (Agirrezabala et al., 2005). In addition, the central domain of the core also undergoes a transition that is probably related to the completion of the DNA packaging.

Despite the fact that the different viral systems present some singular characteristics (probably involved in specific stages of each life cycle), many of the features of the morphogenesis and maturation processes are widely shared among dsDNA bacteriophages, as well as in herpes virus (Ackermann, 1998, 2003; Steven et al., 2005). Evolutionary relationships have been pointed among all of these viruses, but the evolutionary divergence of viral genomes interferes in the detection of presumptive homologies when studied by common sequence-comparison techniques. The bacteriophages infect over 140 bacterial genera, and herpes viruses comprise a family of viruses that infect a wide range of eukaryotic organisms; thus, it is assumed that features such as host recognition and attachment are not shared because they are acquired from each particular host during the specification process (probably by lateral gene transfer). Nevertheless, it has been widely documented that general viral features as the structural components and their basic interactions that yield the shell architecture, as well as the genome-packaging mechanism, have a common structural origin (Bamford et al., 2005). Therefore, although genomes and sequences have diverged, basic architectural designs are maintained. Thus, clear detection of structural folds, and therefore deduction of evolutionary relationships, is still possible by the combination and integration of bioinformatics and structural homology approaches (Zhou et al., 2001). Using this approach, it has been shown that the three-dimensional maps of bacteriophages P22 (Jiang et al., 2003), ϕ29 (Morais et al., 2005), T4 (Fokine et al., 2005), HSV-1 (Baker et al., 2005), and Epsilon15 (Jiang et al., 2006) are consistent with their respective major shell proteins having a core that is HK97 like (Wikoff et al., 2000), thus suggesting that they could have evolved from a common ancestor.

The present study describes the structure of the bacteriophage T7 procapsid shell determined at ~10 Å resolution by cryo-electron microscopy (cryo-EM) in which the signal-to-noise ratio of the reconstruction was maximized by the use of icosahedral symmetry averaging. The combined use of a novel approach to segment and model an average subunit from the electron density map, sequence analysis, and computational homology modeling tools has allowed us to model secondary structure elements of the shell subunit. We obtained a quasi-atomic model for the entire T7 procapsid by fitting a homology model for the capsid subunit gp10 that was based on the atomic structure of HK97. The comparison of this model with the reported prohead structures obtained by cryo-EM (Conway et al., 1995, 2001; Jiang et al., 2003; Morais et al., 2003, 2005) illustrates that T7 may likely adopt the basic HK97-like fold—evidence that the lineage is very broad. The presence of a novel additional domain is proposed to also represent a general feature among these viruses that show both the HK97-like fold and an independent scaffolding-based morphogenetic pathway.

RESULTS

Structure of the T7 Procapsid from Cryo-Electron Microscopy Data

The study of the T7 capsid by using a reconstruction strategy that does not rely on the use of icosahedral symmetry allowed us to generate a three-dimensional reconstruction that, besides the icosahedral shell, revealed the morphology of important internal components, such as the internal scaffold and the core-connector complex (see Agirrezabala et al., 2005). In an attempt to get a higher-resolution structure, the cryo-electron images of isolated procapsids were three-dimensionally reconstructed by using 60-fold, icosahedral symmetry averaging and by maximizing the signal-to-noise ratio and therefore the redundancy for averaging, allowing for a high-resolution analysis of the shell of the viral procapsid structure. Figure 1 shows the reconstructed procapsid after icosahedral averaging. The resolution of the reconstructed volume was found to be 9.8–10.9 Å (according to FSC 0.3 and 0.5 criterion; see Figure S1 in the Supplemental Data available with this article online). The general characteristics are consistent with those described previously at a lower resolution: a T = 7L shell with a diameter of ~510 Å (Cerritelli et al., 2003; Agirrezabala et al., 2005). The capsid shows a very corrugated surface (Figure 1A). The protein gp10 subunits that built the shell are organized into 12 pentamers at the icosahedral five-fold symmetry axes and 60 hexamers that close the icosahedral structure. Three of these hexamers are located on each of the 20 triangular faces of the icosahedral shell (Figure 1A). Sections of the shell revealed a thick wall (up to 50 Å in the wider areas) with an intricate profile (Figure 1B), resulting in a highly corrugated inner surface, with cavities underlying the capsomers and a well-resolved matrix of ridges and crevice-like domains. The conspicuous inner features were also observed at lower resolution, where they were called "nubbins" and were considered as scaffold remnants (Cerritelli et al., 2003). Based on the fact that these features have an identical density to the rest of the shell, and that even after systematic modification of the contour level of the reconstruction we did not detect any consistent contact between the scaffold and the shell, we conclude that these nubbins are in fact part of the shell protein and not scaffolding remnants.

The structure displays a skew arrangement of the hexameric capsomers, and holes are visible in their centers (Figure 1C). The hexamer presents an average diameter of 52 Å and an intercapsomeric distance of 110 Å. These features also agree with those described previously in a lower-resolution analysis (Cerritelli et al., 2003; Agirrezabala et al., 2005). The central cavity in the five-fold symmetric pentamers is only visible at high σ values (above 3σ, while that of the hexamers appears at 1σ) (Figure 1D).

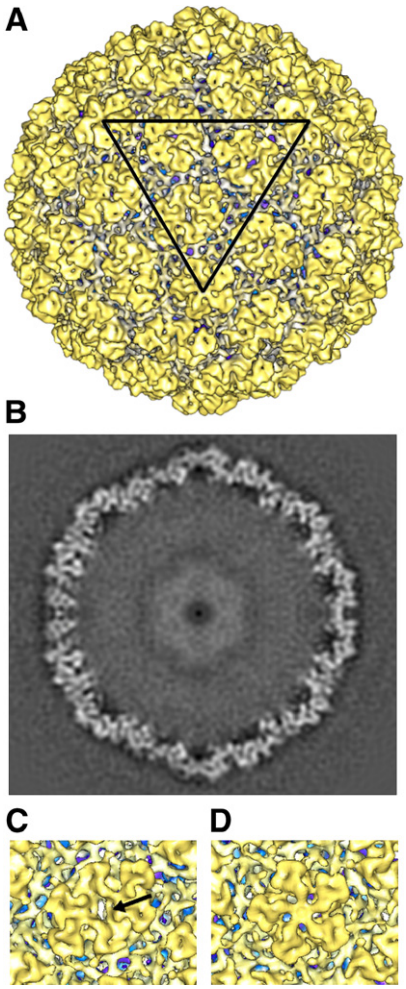

Figure 1. Three-Dimensional Reconstruction

(A) Radially colored volume representation of the three-dimensional reconstructed procapsid. The icosahedral triangular face is indicated.
(B) Plane section of the same view revealing the shell crossprofile.
(C) Enlarged view of the hexamer. The arrow points to hole in the center of the hexamer.
(D) Enlarged view of the pentamer.
The density has been radially color cued with Chimera (Pettersen et al., 2004) and displayed at $\sigma = 2.5$ threshold to enhance the structural features of the reconstructed volume.

Subunit Segmentation in the Experimental Cryo-Electron Microscopy Volumes

The density map of the reconstructed volume at ~10 Å resolution was not sufficient for a clear identification of secondary structural elements, but it did allow for manual segmentation of each of the seven subunits in the asymmetric unit. We employed a novel approach (see Experimental Procedures and Supplemental Data) to iteratively improve this manual segmentation and to align and average the symmetrically independent subunits. Each of the seven subunits, and consequently their average, showed L-shaped morphology, with a globular domain facing the external surface of the capsid and a more extended domain building the inner capsid surface (Figure 2). (Note that the subunits are colored in a consistent way throughout all figures.)

Analysis of the refined orientations of the six hexameric subunits revealed a pseudo two-fold symmetry for the hexamer. The main departure from perfect six-fold symmetry consists of an out-of-plane tilting of monomers 2 (cyan) and 5 (blue), accompanied by a slight elongation of the hexameric structure. Nevertheless, the six structures appear to be very similar, as each monomer in the hexamer has a correlation coefficient of 0.95 or higher with the average density of the remaining five monomers. Calculation of the variance among the six aligned monomers confirmed this high similarity, and it revealed two small areas with increased variability: one in the domain on the outer side of the capsid, and one in the domain on the inner side (see Figure 2C). While the differences in the inner region may still be related to the segmentation procedure (as this area is involved in the interaction between neighboring subunits), those located in the outer region might be attributed to slight conformational adaptation of each of the subunits to the departures from the quasi-identical environment derived from the T = 7 arrangement. The structure of the pentameric subunit may differ more from the hexameric structures, as this subunit has a significantly lower correlation coefficient of 0.88 with the average hexameric subunit.

Structural Model of the T7 Head Subunit gp10A

The structural analysis of the capsid proteins of different viruses reveals surprising relationships. In the case of some double-stranded DNA bacteriophages, such as HK97, T4, P22, ϕ29, and Epsilon15, a picture is emerging that suggests the existence of a common fold that builds the basic subunit of the shell in these viruses (Jiang et al., 2003, 2006; Fokine et al., 2005; Morais et al., 2005). The overall similarity of the structure of the average segmented subunit from the T7 procapsid to the HK97 capsid subunit solved by X-ray crystallography (Wikoff et al., 2000; Helgstrand et al., 2003) prompted us to make a comparison of their amino acid sequences and secondary structures. Although the T7 shell protein gp10A has 345 amino acids, and the mature HK97 gp5 has 280 amino acids (after N-terminal maturation cleavage of its 103 amino-terminal residues), comparison of their sequences showed significant similarities (24% similarity, 10% identity), as shown in Figure 3. This similarity is supported by a more complete sequence alignment among several capsid proteins of viruses belonging to the HK97 and T3/T7 groups (Figure S2), suggesting a close evolutionary relationship among them and a common organization of their secondary structure elements. The main differences are located in the N-terminal domains of both groups of viruses, corresponding to the processed domain (residues 1–103) of HK97 gp5. We then used the structure of HK97 gp5 mature protein to obtain a model for residues Pro76–Glu345 of T7 gp10A by using homology-modeling techniques.

Figure 4 shows the three-dimensional structural model of T7 gp10A based on the structure for the HK97 gp5

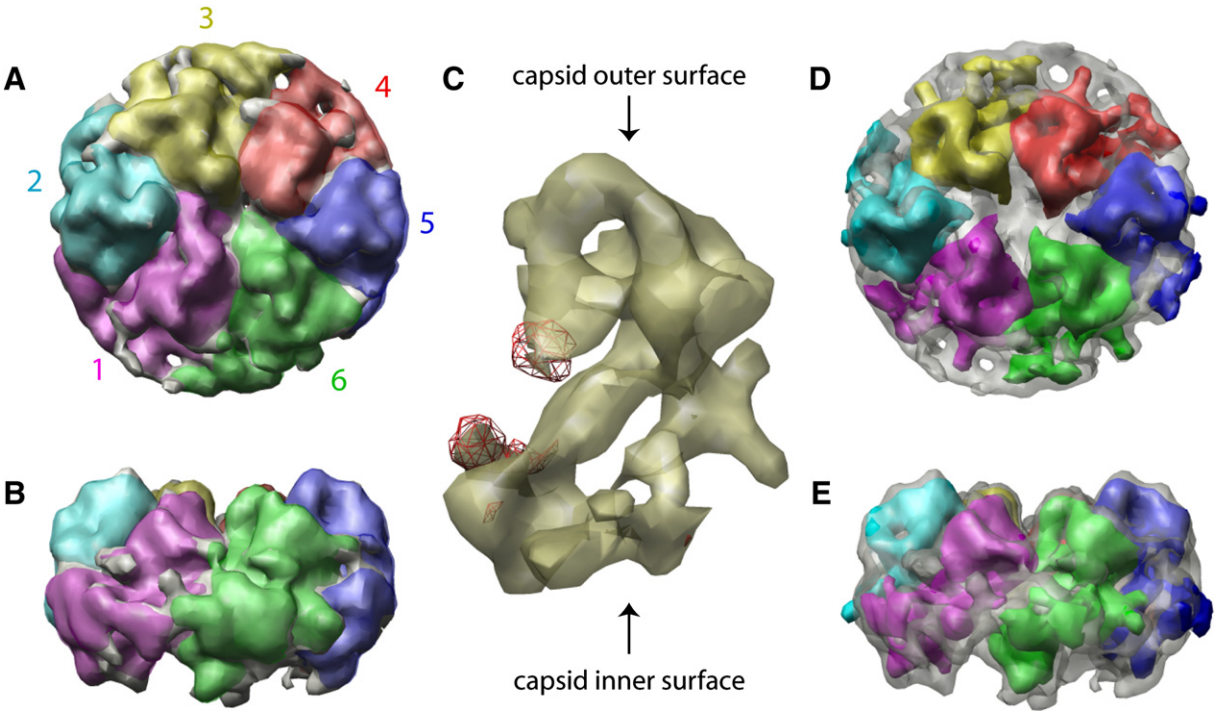

Figure 2. Segmentation and Averaging of the Hexon Subunits

(A and B) Top and side views, respectively, of the initial, manual segmentation of the six hexon subunits (1–6, colored) into the experimental hexon density (gray).

(C) Side view of the average density (yellow) and standard deviation (red) of the six aligned and resegmented hexon monomers. The orientation of the subunit with respect to the capsid surface is indicated (capsid outer and inner surfaces).

(D and E) Top and side views, respectively, of six copies of the aligned average hexon density (colored) into the experimental hexon density (gray).

protein (PDB: 1OHG) (Helgstrand et al., 2003), used as template. Following the nomenclature described for gp5 (Wikoff et al., 2000), the model for gp10 (residues 76–345) consists of domain A (residues 205–294 and 336–345), domain P (residues 106–117, 152–205, and 295–335), the E loop (residues 118–151), and an unstructured N-terminal arm (residues 76–105). The A domain includes α helices H2 and H3 and an additional small β sheet. The P domain contains the long H1 helix as well as an elongated three-stranded β sheet. The main difference between the homology model and its template is the predicted shorter length of H1 and H2 of gp10A.

Fitting of the gp10 Model into the Averaged T7 Subunit Volume

The homology model for gp10A was fitted into the electron density of the averaged hexon subunit. The improved signal-to-noise ratio of this average, the similarity of the different subunits derived either from the hexamer or the pentamer, and the limited resolution of our map ($\sim$10 Å) support the working assumption that the averaged subunit can accommodate the seven quasi-equivalent variants of gp10A.

After computational fitting of the entire homology model, it was observed that a hinge movement of $\sim$15° between domains A and P could better accommodate the model to the experimental volume. Therefore, a manual fitting was performed considering domains A (amino acids 202–295 and 337–345) and P (amino acids 100–117, 152–201, and 296–336) separately. The position of the loop comprising residues 202–216 required further adjustment to account for the density in front of H3. Furthermore, the E loop (amino acids 118–151) was removed from the model, as no potential density was observed for it in the averaged experimental map. Subsequently, the initially positioned domains A and P were computationally refined for better fitting by using COLACOR from Situs (Wriggers and Birmanns, 2001) and were reconnected, and the entire model was subjected to energy minimization with Refmac (Murshudov et al., 1999). The result of the entire procedure is shown in Figure 5. The same steps were repeated to fit the gp10 model into the density of one of the penton capsomers, and only minor differences with respect to the fitting of the averaged hexon capsomer were obtained (data not shown).

Figure 5 shows two views from the fitted model. Domain A clearly fits into the external area of the L-shaped procapsid subunit. The H2 and H3 helices map well into the structural features of this region, while the H1 helix of domain P fits into the long rod of the basal domain of the subunit, facing the interior of the capsid. The three-stranded, antiparallel β sheet, flanking H1, also fits nicely into the basal

Figure 3. Sequence Alignment of HK97 and T7 Capsid Proteins

HK97_gp5, bacteriophage HK97 major capsid protein gp5; T7_gp10A, bacteriophage T7 major capsid protein 10A. Alignment is shadowed according to conservation. Secondary structure elements of the HK97 major capsid protein structure (HK97_gp5_ss) used as template (PDB: 1OHG) and the proposed model for T7 gp10A protein (T7_gp10A_ss) are also indicated (H, α helix; E, β strand). Positions of HK97 residues Lys169 and Asn356 involved in subunit crosslinking are indicated (*).

area of the L-shaped subunit. Besides minor misadjustments of small loops in domain A, the main features that are not fitted into the experimental subunit density are the E loop and the N-terminal 100 amino acids of gp10A, whose sequence is absent in the gp5 template.

Fitting the gp10 Model into the Isolated Pentamer and Hexamer

In order to understand the relationships between the subunits building the isolated hexamer and pentamer, we performed an intermediate rigid fitting step. We used the alignment transformations resulting from the previous iterative segmentation procedure for the averaged capsomer, and we translated the atomic coordinates of the fitting into one segmented pentamer and one segmented hexamer (Figure 6). The model hexamer (Figure 6A) reproduces well the main morphological features of the segmented experimental hexamer (Figures 6C and 6E; Figure S3), including the open channel in the center of the capsomer. The subunits (color coded to allow for comparison with the original segmentation shown in Figure 2) show extensive lateral contacts, but they are not heavily interlaced. These intermediate fitting results were then used to calculate a difference map between the segmented, experimental hexamer density and the model hexamer, truncated at 10 Å resolution. The areas with the largest differences (at a level of 3 standard deviations) were found at the lower side of the subunit, below domain P and facing the interior of the viral procapsid (Figure 6E, highlighted in magenta).

In the case of the pentamer, the model based on the assembly of the averaged subunit also matches the experimental density well, showing a more compact capsomer assembly, except in the areas below domain P, in which significant differences were located. Again, as in the case of the hexamer, these areas were found facing the interior of the capsid (Figures 6B, 6D, and 6F). Due to the fact that the average volume corresponding to these differential regions (10,000 A^3) could accommodate a protein moiety around 83 amino acids (assuming an average density value for proteins of ~1.33 g/mol), and although this extra density could partly accommodate the E loop, it is tempting to suggest that this difference volume is occupied by the 100 amino acids of the amino terminus of gp10 that are also missing in template gp5 from HK97.

An interesting feature is derived from the analysis of the electrostatic potential of our models for the hexamer and pentamer by using Delphi (Rocchia et al., 2001, 2002). We found that the inner face of these capsomers shows an overall negative surface charge, both in the case of the pentamer and the hexamer (Figure 7). A similar charge distribution was found in the inner surface of prohead II from HK97 (Conway et al., 2001). Even if we consider the presence of the additional density from the

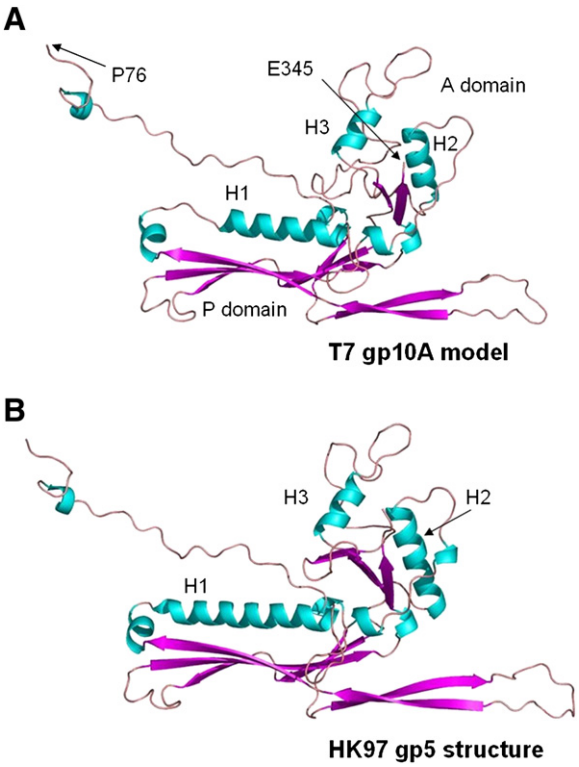

Figure 4. Structure Model for T7 gp10A Protein

(A) Three-dimensional modeled structure for T7 major capsid protein gp10A. Location of α helices H1, H2, and H3, the position of residues Pro76 and Glu345 (N and C ends, respectively, of the modeled sequence), and the putative location of proposed A and P domains, as well as the N-terminal arm and E loop, are indicated.

(B) Structure of HK97 major capsid protein gp5 (PDB: 1OHG) used as template for the modeling of T7 capsid protein. The position of equivalent H1, H2, and H3 helices is also depicted.

experimental shell reconstruction (that we have tentatively assigned to the amino-terminal region of gp10), the general negative character of the capsomer inner surface is not substantially altered (see Figure S4).

Fitting the gp10 Model into the Entire Virus Capsid

The intermediate fitting results with the pentamer and hexamer described above were used to build an initial model for the entire asymmetric unit for the procapsid shell. This model was subjected to refinement by using the icosahedral symmetry option in URO (Navaza et al., 2002). For this purpose, as the first 100 amino-terminal residues are absent in our model, we also removed the densities assigned to these residues from the experimental density map.

Visual inspection of the refined atomic model confirmed a good overall fitting into the density, in general avoiding clashes between capsomers and between loops. The final pseudo atomic model for the entire procapsid shell is shown in Figure 8A. The crosscorrelation coefficient (CCC) for the entire fitting of the capsid improved from 0.64 in our intermediate results to a final value of 0.67, according to URO. These CCCs were computed on the map used for the fitting (that had the densities assigned to the 100 first amino acids removed). When using a mask with the shape of the fitted densities, the so-called local cross-correlation coefficient (LCCC) improved from 0.80 to a final 0.83 during URO refinement.

The general occupancy of the experimental data by the pseudo atomic model is good, and the seven different subunits building the asymmetric unit of the icosahedral shell fill up the experimental volume evenly. Only minor differences emerge between the model and the experimental density map, but some of them are noteworthy. The difference map between the experimental density and our pseudo atomic model, truncated at 10 Å and thresholded at 2 standard deviations, shows three areas around the icosahedral three-fold axes that might be important for the stabilization of the contacts among capsomers, leading to the stabilization of the procapsid structure (Figures 8B–8D). The area around the three-fold axis built by three identical subunits, each from a different hexamer (Figure 8B), shows the presence of three rods of electron density around the symmetry axis that are not explained by our model for gp10. These rods (colored red in Figure 8B) connect each of the three subunits with the neighboring subunit, following a trajectory from inside the capsid to the outside. Due to their size, shape, and position with respect to the subunit domain, it is tempting to suggest that the E loop of each subunit fills each of the rods (Figure 8B, dashed lines). In this way, the E loop of each subunit would cross over domain P of its neighbor, leading to a contact threading among the capsomers (as a molecular swapping) in a way similar to that described for HK97 (Wikoff et al., 2000). We have found a similar triangle of E loops around the two other types of interactions among three different subunits from different hexamers (Figure 8C), and in the case of the hexamer-pentamer interaction (Figure 8D).

DISCUSSION

The presence of a common fold in the major capsid protein from several unrelated bacteriophages has been suggested based on structural evidence obtained by X-ray crystallography of HK97 (Wikoff et al., 2000) and by cryo-EM of P22 (Jiang et al., 2003), ϕ29 (Morais et al., 2005), or Epsilon15 (Jiang et al., 2006). The atomic structure of the T4 pentavalent capsid protein gp24 has confirmed this hypothesis (Fokine et al., 2005). In addition, the cryo-EM reconstruction of HSV-1 capsid (Baker et al., 2005) showed that herpes virus probably shares the basic HK97-like architecture in the floor domain of its shell capsid protein. In a similar way as the classical "jelly-roll" β sandwich fold found in many eukaryotic viruses, the HK97-like fold might therefore be considered as a characteristic signature for another class of viruses (for reviews in viral folds, see Chapman and Liljas, 2003; Reddy and Johnson, 2005). Based on a structural classification of viral capsid proteins, it has been recently proposed that all viral lineages could be divided into three structurally related

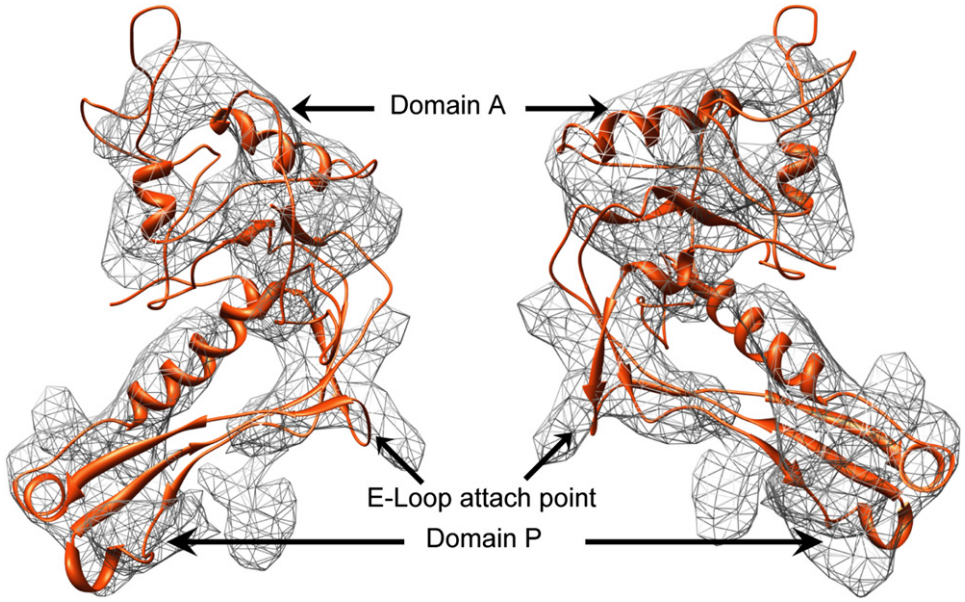

Figure 5. Final Model for T7 Capsid Protein gp10A after Fitting into the Electron Density of the Average Hexon Subunit
Two different views are shown; the density threshold is at ~2 standard deviations. The E loop is omitted, as no hints for the corresponding density are observed in the average.

major groups spanning all life domains, PRD-like, BTV-like, and HK97-like groups (Bamford et al., 2005).

In this study, we have obtained a cryo-EM reconstruction of the T7 procapsid shell at ~10 Å resolution. Initial, manual segmentation of the individual procapsid subunits from this map was improved by a novel procedure, in which all independent subunits were iteratively aligned with respect to their average density, and inspection of the aligned subunits served to improve the segmentation. The resulting average density for the segmented subunits showed a high similarity to the atomic model of HK97 gp5 (Wikoff et al., 2000), which prompted us to employ homology modeling and subsequent fitting of the resulting atomic model in the cryo-EM density. In this way, we obtained a quasi-atomic model for the T7 procapsid shell.

The homology model for gp10A comprises the A and P domains that form the compact core of the HK97-like fold. The good fit of this quasi-atomic model with the cryo-EM density (Figure 5) is an indication of the quality of the homology modeling performed. A comparison of this model with the HK97 template structure reveals a high similarity in the overall architecture of these proteins, with highly conserved relative positions of the A and P domains. Two relatively flexible domains of HK97 are absent in the homology model: the E loop and the N-terminal domain. In HK97, the E loop forms an extended two-stranded β sheet, while the N-terminal domain has very little homology with that of T7 gp10. Still, we were able to infer the possible location of the N-terminal domain and the orientation of the E loop from difference maps between the cryo-EM density and the quasi-atomic model. The 100 residues of the gp10A N-terminal domain were putatively assigned to the electron density region on the inner side of the shell (Figure 6), and the E loops were assigned to fill rods of difference density in a triangular arrangement that was observed for three independent capsomeric interfaces (Figure 8).

Although the T7 shell protein gp10 is mainly produced as a 345 amino acid form (gp10A), 10% of gp10 (called gp10B) has a C-terminal extension of 52 amino acids, which are the product of a readthrough of the gp10 gene. Nevertheless, the absence of gp10 frame shifting results in capsids that are entirely built by gp10A, which are as stable as wild-type capsids (Condron et al., 1991). On the other hand, as no information on the topological distribution of gp10B is available, we have tried to locate this protein by difference imaging between the quasi-atomic icosahedral model as obtained in this study and the previously determined nonicosahedral reconstructions of T7 procapsids (EMD-1161 and EMD-1162; see Agirrezabala et al., 2005). Unfortunately, no major differences that would hint at the localization of gp10B were found, probably due to the limited resolution of the nonicosahedral maps (data not shown).

The proposed intersubunit interactions in the quasi-atomic T7 procapsid model are very similar to those reported for the quasi-atomic model of HK97 procapsid II (Wikoff et al., 2000). In particular, the molecular interactions around the (quasi) three-fold symmetry axes show striking similarities (Figure 8). The interaction between the P domain of one subunit and the E loop of the neighboring one in T7 leads to an interlocking of the subunits. In the case of HK97, the topology of the interaction is similar, although, in this case, after shell maturation it is further secured by a chemical crosslink between Asn356 of the P domain and Lys169 in the neighboring E loop (Wikoff et al.,

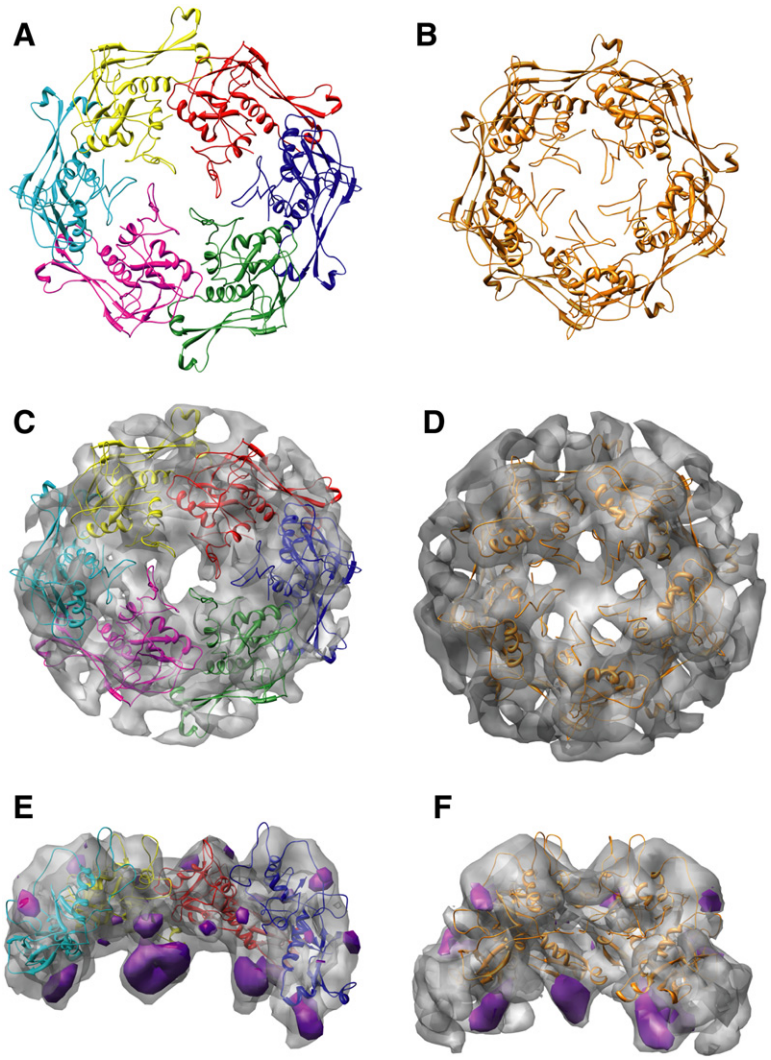

Figure 6. Intermediate Models for the Hexon and Penton

(A) Hexon structure in simplified ribbon representation. Each monomer is shown in a different color, with the same code as in Figure 2.

(B) Penton structure in simplified ribbon representation. All monomers are shown in orange.

(C) Top view of the hexon structure fitted into the electron density. The density threshold is selected to represent 100% of the hexon mass.

(D) Same figure as (C), but for the penton.

(E) Front segmented view of the hexon structure fitted into the electron density. Clear masses attributable to the amino-terminal domain of gp10A can be observed at the inner side of the difference map (3 standard deviations, magenta).

(F) Same figure as (E), but for the penton.

2000). While the noncovalent interlocking of subunits seems to suffice in T7, the slight destabilization induced by the capsid expansion during maturation in HK97 requires a compensation thorough the covalent crosslinking of domain P and the E loop (Ross et al., 2005).

Also, the distribution of the charges on the surface of the subunits is equivalent, with a clear, net negative, electrostatic potential in the inner capsid surface (Figure 7). This potential would result in an electrostatic repulsion of the negatively charged DNA during the packaging process. This pressure, in equilibrium with bending forces (Tzlil et al., 2003), may result in the experimentally observed spool arrangement of the packaged DNA (Cerritelli et al., 1997; Agirrezabala et al., 2005).

The generic maturation pathway of most of the tailed dsDNA bacteriophages, as well as herpes virus, shows

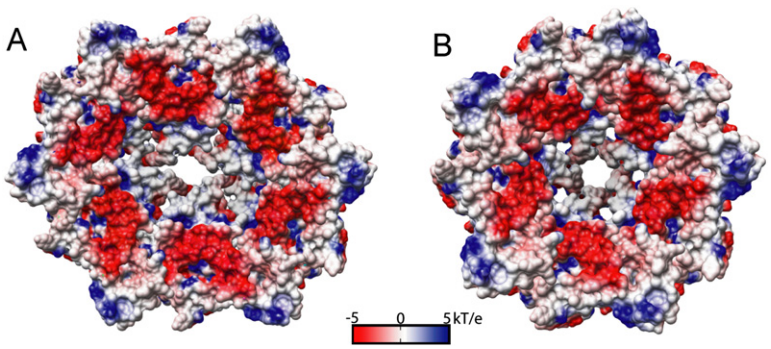

Figure 7. Internal Surface Potential

(A) Bottom view of the hexon surface (view from inside the capsid) showing an overall negative electrostatic potential.

(B) Same figure as (A), but for the penton.

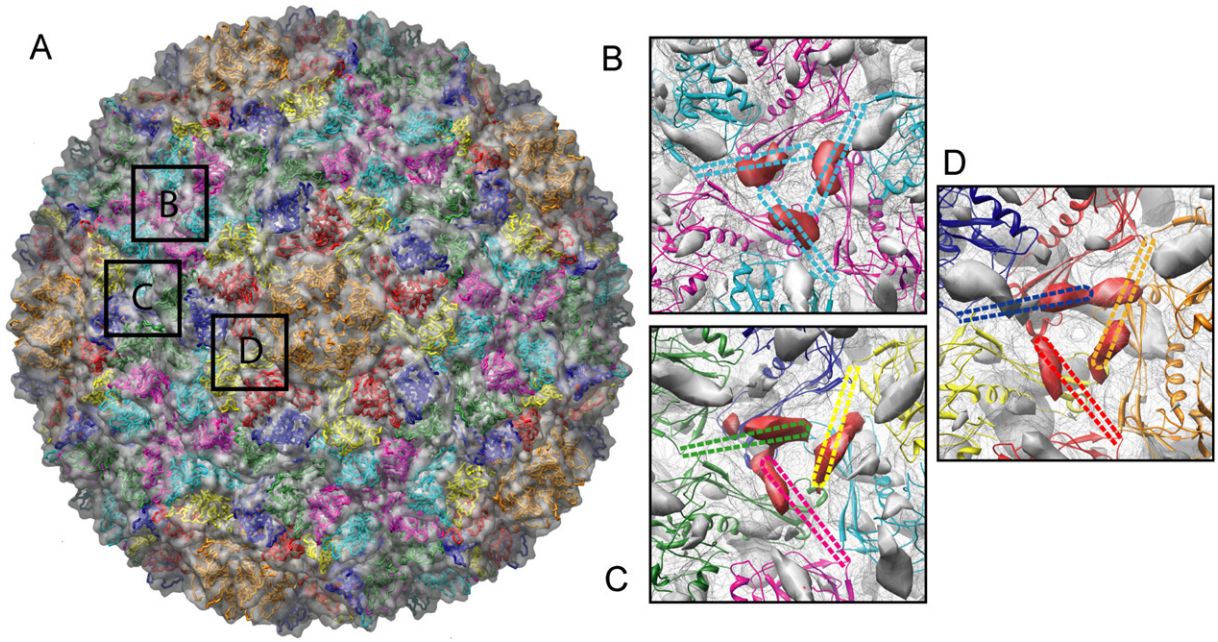

Figure 8. Final Model for the Arrangement of Protein gp10A into the Entire T7 Procapsid

(A) Entire shell representation, obtained after refining the fitting of models in Figure 6 imposing icosahedral symmetry. Each monomer is shown in a different color, with the same code as in Figures 2 and 6.

(B) Detail of the pseudo three-fold axis involving three identical monomers of type 2. The difference map at 2 standard deviations is shown in solid gray, and the masses attributed to E loops are colored red.

(C) Detail of the pseudo three-fold axis, involving monomers of types 1, 3, and 6. The masses of the E loops (colored in red) are also clearly visible.

(D) Detail of a third pseudo three-fold axis involving monomers of types 4 and 5 of the hexon and one from the penton. The masses of the E loops are also clearly visible. The E loop segment from each model subunit has been shown schematically as a dotted hairpin colored according to the type of subunit. The superposition of the schematic E loop and the corresponding masses derived from the experimental data (colored in red) are consistent in the three types of pseudo three-fold axes.

extensive homologies. Nevertheless, there are important differences between bacteriophage HK97 and the rest of the phages. In addition to the presence of the crosslinking-stabilizing mechanism (Ross et al., 2005), another important difference is the absence of a scaffolding protein in the HK97 system. It has been proposed that the proteolyzed N-terminal 103 amino acids (a proteolytic event that takes place during the PI-to-PII prohead transition) might play this role during the initial stages of the shell assembly of phage HK97 (Conway et al., 1995). Phages T7, P22, or ϕ29, as the majority of the phages, present an independent scaffolding protein, essential for the correct assembly of the proheads (for a review, see Dokland, 1999). In many cases, including phage T7, the gene coding for this protein is located upstream of the capsid protein gene. Several reports have suggested the existence of a common motif between the N-terminal 33 amino acids of the ϕ29 scaffolding protein (gp7) (Morais et al., 2003) and the C-terminal coat protein-binding domain of the phage P22 scaffolding protein (Sun et al., 2000). It is noteworthy that the alignment of the Δ domain 103 residues of HK97 gp5 with the sequence of the T7 scaffolding protein shows a high homology profile, a homology extending to other scaffolding proteins from other phages, such as gp7 from ϕ29, gp7 from phage B103, and the capsid assembly protein from phage ϕA1122 (see Figure S5). A conspicuous coiled-coil structure, a dimer comprising two long α helices coiled with two smaller ones, appears to be a common structural motif in all of these scaffolding proteins, supporting this presumptive role of the Δ domain in the immature HK97 gp5.

The presence of two independent proteins for the cooperative construction of virus shells is a clear evolutionary advantage, offering improved flexibility and control (Steven et al., 2005). On the other hand, it requires specific domains to interact with each other. Comparison of several major shell proteins from other phages with the HK97 capsid protein gp5 has served to locate the additional density that accounts for the residues that are not present in the smaller HK97 protein (containing 281 amino acids). For bacteriophage P22 gp5 (429 amino acids) and phage ϕ29 gp8 (448 amino acids) for example, this additional density, whose role is still unclear, was shown to be located at the external face of the viral shell, just above the equivalent to the HK97 E loop (Jiang et al., 2003; Morais et al., 2005). However, in the case of T7, we observe additional density that could accommodate the N-terminal 100 residues of gp10A at the inner surface of the procapsid. The fact that the phage T7 internal additional domain (the major difference between T7 and HK97 shell proteins) is located in the same place at which the Δ domain is placed in HK97 procapsid I (Conway et al., 1995)

suggests that the T7 extra domain could be involved in the interaction with the scaffolding lattice extensions during virus assembly. Also, in the case of P22, an additional density is located in a similar position as that in T7 (Jiang et al., 2003). This density corresponds to a long helix (H0) present in the procapsid that was not seen in the mature phage. This possible refolding event indicated that this region could no longer be required in the mature virus, and it was proposed that it could somehow be involved in some step of shell stabilization. We suggest that the T7 additional domain (comprising the N-terminal 100 residues) could be equivalent to the P22 procapsid helix H0 region. A possible mechanism for the maturation transitions could be that, as long as the additional internal domain is placed in the inner part of the shell and is connected to the main scaffolding lattice, it might act as a stabilizing link preventing the premature rearrangement of the subunit to its mature state. Once the DNA-packaging mechanism would be activated, the following disassembly of the scaffolding lattice would disrupt all of the connections between both structures and induce the structural rearrangements of the capsid protein that lead to the mature virion, together with a release of the scaffolding protein subunits by a hitherto unknown mechanism.

The model proposed here for the T7 procapsid shell involves a number of precise interactions between different domains of the shell subunits. Although the definition of the detailed residues involved in such interactions will depend upon the generation of higher-resolution models, there are several aspects that can be tested in the near future. The predicted role of the interaction of the E loop and the P domain in the stabilization of the shell can be analyzed by testing the effect of gp10A mutants with partially truncated E loops on particle stability by using different biophysical approaches (scanning calorimetry, force microscopy, etc. [Galisteo and King, 1993; Ivanovska et al., 2004; Ross et al., 2005]). Also, further studies involving higher-resolution cryo-EM analysis of different viral structures, including the mature T7 virion, and mainly the production of corresponding atomic structures, will be required to get a more detailed picture of how the viral maturation process occurs at the molecular level.

EXPERIMENTAL PROCEDURES

Sample Preparation

Type I procapsids were purified from *E. coli* lysates of BL21 cells infected with a mutant in the viral DNA polymerase (gp5) as previously described (Agirrezabala et al., 2005).

Electron Microscopy and Image Processing

The experimental approach for image acquisition and processing has been previously described (Agirrezabala et al., 2005). Briefly, low-dose images of purified procapsids were taken on an FEI TecnaiG^2 FEG200 electron cryo-microscope at 200 kV by using a nominal magnification of 50,000×. The selected micrographs were scanned with a step size of 14 μm on a Zeiss scanner (Photoscan TD,Z/I Imaging Corporation). The final pixel size corresponds to 2.72 Å/pixel. A total of 4460 particles were used and preprocessed to normalize mean intensities and variances and to remove linear background gradients. The three-dimensional projection alignment procedure (real space projection matching) with correction of the contrast transfer function (CTF) in defocus groups, varying the defocus of the selected images from 1 to 3 μm, was used. The enhancement of the high-resolution Fourier amplitudes was done by using X-ray data from HK97 capsid protein (PDB: 1OHG) (Helgstrand et al., 2003). Refinement convergence was deemed to be reached when >95% of the experimental images most closely resembled the same reference projection as they had in the previous step. The previously presented icosahedral reconstruction of the procapsid (Agirrezabala et al., 2005) at low resolution (20 Å) was used as the initial three-dimensional reference. The final resolution of the reconstructed procapsid was 9.8 Å and 10.9 Å, determined by the FSC 0.3 and 0.5 criterions, respectively (see Figure S1). The hand of the volume was assumed to be the same as that defined for previously presented volumes (Cerritelli et al., 2003). Data processing was performed by using the SPIDER image-processing system (Frank et al., 1996). The volume has been deposited in the 3D-EM database with accession code EMD-1321.

Segmentation and Structural Analysis

The first step in the segmentation of the individual subunits was the isolation of the hexamers and the pentamers from the original volume by using spherical masks generated and applied with Xmipp tools (Sorzano et al., 2004). The molecular envelopes of individual subunits were then determined by visual inspection of the density displayed at different σ levels (described in Morais et al., 2005; Supplemental Data). The Amira Segmentation Editor (http://amira.zib.de) was used for the manual isolation of the different subunits. The segmented envelopes were then converted into masks by using raised cosine edges to generate soft transitions between subunits, and they were applied to the original complete volume by using Xmipp tools, which isolated the different subunits for further improvement as described in Figure S2 and the corresponding legend.

Amino Acid Sequence Alignment and Molecular Modeling

Homologous sequences to T7 gp10A in protein databases were obtained by using Blast (Altschul et al., 1990). Members of the T3/T7 and HK97 families were aligned with ClustalW (Thompson et al., 1994) and T-COFFEE algorithms (Notredame et al., 2000). The structural model for capsid protein gp10A of T7 virus (SwissProt code: VC10A_BPT7-P19726) was built by using homology modeling procedures based on multiple structure-based amino acid sequence alignments of capsid proteins of viruses belonging to HK97 and T3/T7 groups and the crystallographic coordinates of HK97 major capsid protein gp5 (Protein Data Bank [PDB] entry: 1OHG) (Helgstrand et al., 2003). For the fitting, the T7 gp10A domains were considered as follows: A domain (residues 202–295, 337–345), P domain (residues 100–117, 152–201, 296–336), and E loop (residues 118–151). The three-dimensional model was built by using the SWISS-MODEL server (Guex and Peitsch, 1997; Peitsch, 1996; Schwede et al., 2003) facilities at http://www.expasy.ch/swissmod/SWISS-MODEL.html, and their structural quality was checked by using the WHAT-CHECK routines (Hooft et al., 1996) from the WHAT IF program (Vriend, 1990) from the same server. Finally, in order to optimize geometry, release local constraints, and correct possible bad contacts, the modeled structure was energy minimized with the implementation of the GROMOS 43B1 force field in the program DeepView (Guex and Peitsch, 1997), by using 500 steps of steepest descent minimization, followed by 500 steps of conjugate-gradient minimization.

Supplemental Data

Supplemental Data as described in the text, including five figures, are available at http://www.structure.org/cgi/content/full/15/4/461/DC1/.

ACKNOWLEDGMENTS

We acknowledge the help during different parts of this work of Daniel Luque, Roberto Miranda, Jaime Martín-Benito, Javier Chichón, and Jose Maria Valpuesta, as well as the critical comments from

A.C. Steven. This work was supported by grants BFU-2005-06487 from the Spanish Ministerio de Educación y Ciencia, S-0505/MAT-0283 from the DG Universidades e Investigacion from the Comunidad de Madrid and by the contract NoE LSHG-2004-502828 from the European Union. The work at the Centro de Biología Molecular Severo Ochoa was supported by grant SAF2004-06843 from the Spanish Ministerio de Educación y Ciencia, Centros de Investigación Biomédica en Red C03/2006/0026 from the Spanish Ministerio de Sanidad, and by an institutional grant of "Fundación Ramón Areces."

Received: December 11, 2006
Revised: February 19, 2007
Accepted: March 13, 2007
Published: April 17, 2007

REFERENCES

Ackermann, H.W. (1998). Tailed bacteriophages: the order caudovirales. Adv. Virus Res. *51*, 135–201.

Ackermann, H.W. (2003). Bacteriophage observations and evolution. Res. Microbiol. *154*, 245–251.

Agirrezabala, X., Martin-Benito, J., Caston, J.R., Miranda, R., Valpuesta, J.M., and Carrascosa, J.L. (2005). Maturation of phage T7 involves structural modification of both shell and inner core components. EMBO J. *24*, 3820–3829.

Altschul, S.F., Gish, W., Miller, W., Myers, E.W., and Lipman, D.J. (1990). Basic local alignment search tool. J. Mol. Biol. *215*, 403–410.

Baker, M.L., Jiang, W., Rixon, F.J., and Chiu, W. (2005). Common ancestry of herpesviruses and tailed DNA bacteriophages. J. Virol. *79*, 14967–14970.

Bamford, D.H., Grimes, J.M., and Stuart, D.I. (2005). What does structure tell us about virus evolution? Curr. Opin. Struct. Biol. *15*, 655–663.

Cerritelli, M.E., Cheng, N., Rosenberg, A.H., McPherson, C.E., Booy, F.P., and Steven, A.C. (1997). Encapsidated conformation of bacteriophage T7 DNA. Cell *91*, 271–280.

Cerritelli, M.E., Conway, J.F., Cheng, N., Trus, B.L., and Steven, A.C. (2003). Molecular mechanisms in bacteriophage T7 procapsid assembly, maturation and DNA containment. In Advances in Protein Chemistry, W. Chiu and J.E. Johnson, eds. (San Diego, CA: Academic Press), pp. 301–323.

Chapman, M.S., and Liljas, L. (2003). Structural folds of viral proteins. Adv. Protein Chem. *64*, 125–196.

Condron, B.G., Atkins, J.F., and Gesteland, R.F. (1991). Frameshifting in gene 10 of bacteriophage T7. J. Bacteriol. *173*, 6998–7003.

Conway, J.F., Duda, R.L., Cheng, N., Hendrix, R.W., and Steven, A.C. (1995). Proteolytic and conformational control of virus capsid maturation: the bacteriophage HK97 system. J. Mol. Biol. *253*, 86–99.

Conway, J.F., Wikoff, W.R., Cheng, N., Duda, R.L., Hendrix, R.W., Johnson, J.E., and Steven, A.C. (2001). Virus maturation involving large subunit rotations and local refolding. Science *292*, 744–748.

Dokland, T. (1999). Scaffolding proteins and their role in viral assembly. Cell. Mol. Life Sci. *56*, 580–603.

Dunn, J.J., and Studier, F.W. (1983). Complete nucleotide sequence of bacteriophage T7 DNA and the locations of T7 genetic elements. J. Mol. Biol. *166*, 477–535.

Fokine, A., Leiman, P.G., Shneider, M.M., Ahvazi, B., Boeshans, K.M., Steven, A.C., Black, L.W., Mesyanzhinov, V.V., and Rossmann, M.G. (2005). Structural and functional similarities between the capsid proteins of bacteriophages T4 and HK97 point to a common ancestry. Proc. Natl. Acad. Sci. USA *102*, 7163–7168.

Frank, J., Radermacher, M., Penczek, P., Zhu, J., Li, Y., Ladjadj, M., and Leith, A. (1996). SPIDER and WEB: processing and visualization of images in 3D electron microscopy and related fields. J. Struct. Biol. *116*, 190–199.

Fujisawa, H., and Morita, M. (1997). Phage DNA packaging. Genes Cells *2*, 537–545.

Galisteo, M.L., and King, J. (1993). Conformational transformations in the protein lattice of phage P22 procapsids. Biophys. J. *65*, 227–235.

Guasch, A., Pous, J., Ibarra, B., Gomis-Ruth, F.X., Valpuesta, J.M., Sousa, N., Carrascosa, J.L., and Coll, M. (2002). Detailed architecture of a DNA translocating machine: the high-resolution structure of the bacteriophage ϕ29 connector particle. J. Mol. Biol. *315*, 663–676.

Guex, N., and Peitsch, M.C. (1997). SWISS-MODEL and the Swiss-PdbViewer: an environment for comparative protein modeling. Electrophoresis *18*, 2714–2723.

Helgstrand, C., Wikoff, W.R., Duda, R.L., Hendrix, R.W., Johnson, J.E., and Liljas, L. (2003). The refined structure of a protein catenane: the HK97 bacteriophage capsid at 3.44 Å resolution. J. Mol. Biol. *334*, 885–899.

Hooft, R.W., Vriend, G., Sander, C., and Abola, E.E. (1996). Errors in protein structures. Nature *381*, 272.

Ivanovska, I.L., de Pablo, P.J., Ibarra, B., Sgalari, G., MacKintosh, F.C., Carrascosa, J.L., Schmidt, C.F., and Wuite, G.J. (2004). Bacteriophage capsids: tough nanoshells with complex elastic properties. Proc. Natl. Acad. Sci. USA *101*, 7600–7605.

Jiang, W., Li, Z., Zhang, Z., Baker, M.L., Prevelige, P.E., Jr., and Chiu, W. (2003). Coat protein fold and maturation transition of bacteriophage P22 seen at subnanometer resolutions. Nat. Struct. Biol. *10*, 131–135.

Jiang, W., Chang, J., Jakana, J., Weigele, P., King, J., and Chiu, W. (2006). Structure of epsilon15 bacteriophage reveals genome organization and DNA packaging/injection apparatus. Nature *439*, 612–616.

Matsuo-Kato, H., Fujisawa, H., and Minagawa, T. (1981). Structure and assembly of bacteriophage T3 tails. Virology *109*, 157–164.

Morais, M.C., Kanamaru, S., Badasso, M.O., Koti, J.S., Owen, B.A., McMurray, C.T., Anderson, D.L., and Rossmann, M.G. (2003). Bacteriophage phi29 scaffolding protein gp7 before and after prohead assembly. Nat. Struct. Biol. *10*, 572–576.

Morais, M.C., Choi, K.H., Koti, J.S., Chipman, P.R., Anderson, D.L., and Rossmann, M.G. (2005). Conservation of the capsid structure in tailed dsDNA bacteriophages: the pseudoatomic structure of phi29. Mol. Cell *18*, 149–159.

Morita, M., Tasaka, M., and Fujisawa, H. (1995). Structural and functional domains of the large subunit of the bacteriophage T3 DNA packaging enzyme: importance of the C-terminal region in prohead binding. J. Mol. Biol. *245*, 635–644.

Murshudov, G.N., Vagin, A.A., Lebedev, A., Wilson, K.S., and Dodson, E.J. (1999). Efficient anisotropic refinement of macromolecular structures using FFT. Acta Crystallogr. D Biol. Crystallogr. *55*, 247–255.

Navaza, J., Lepault, J., Rey, F.A., Alvarez-Rua, C., and Borge, J. (2002). On the fitting of model electron densities into EM reconstructions: a reciprocal-space formulation. Acta Crystallogr. D Biol. Crystallogr. *58*, 1820–1825.

Notredame, C., Higgins, D.G., and Heringa, J. (2000). T-Coffee: a novel method for fast and accurate multiple sequence alignment. J. Mol. Biol. *302*, 205–217.

Peitsch, M.C. (1996). ProMod and Swiss-Model: internet-based tools for automated comparative protein modelling. Biochem. Soc. Trans. *24*, 274–279.

Pettersen, E.F., Goddard, T.D., Huang, C.C., Couch, G.S., Greenblatt, D.M., Meng, E.C., and Ferrin, T.E. (2004). UCSF Chimera–a visualization system for exploratory research and analysis. J. Comput. Chem. *25*, 1605–1612.

Reddy, V.S., and Johnson, J.E. (2005). Structure-derived insights into virus assembly. Adv. Virus Res. *64*, 45–68.

Rocchia, W., Alexov, E., and Honig, B. (2001). Extending the applicability of the nonlinear Poisson-Boltzmann equation: multiple dielectric constants and multivalent ions. J. Phys. Chem. B *105*, 6507–6514.

Rocchia, W., Sridharan, S., Nicholls, A., Alexov, E., Chiabrera, A., and Honig, B. (2002). Rapid grid-based construction of the molecular surface and the use of induced surface charge to calculate reaction field energies: applications to the molecular systems and geometric objects. J. Comput. Chem. *23*, 128–137.

Ross, P.D., Cheng, N., Conway, J.F., Firek, B.A., Hendrix, R.W., Duda, R.L., and Steven, A.C. (2005). Crosslinking renders bacteriophage HK97 capsid maturation irreversible and effects an essential stabilization. EMBO J. *24*, 1352–1363.

Schwede, T., Kopp, J., Guex, N., and Peitsch, M.C. (2003). SWISS-MODEL: an automated protein homology-modeling server. Nucleic Acids Res. *31*, 3381–3385.

Serwer, P. (1976). Internal proteins of bacteriophage T7. J. Mol. Biol. *107*, 271–291.

Simpson, A.A., Tao, Y., Leiman, P.G., Badasso, M.O., He, Y., Jardine, P.J., Olson, N.H., Morais, M.C., Grimes, S., Anderson, D.L., et al. (2000). Structure of the bacteriophage phi29 DNA packaging motor. Nature *408*, 745–750.

Sorzano, C.O., Marabini, R., Velazquez-Muriel, J., Bilbao-Castro, J.R., Scheres, S.H., Carazo, J.M., and Pascual-Montano, A. (2004). XMIPP: a new generation of an open-source image processing package for electron microscopy. J. Struct. Biol. *148*, 194–204.

Steven, A.C., Trus, B.L., Maizel, J.V., Unser, M., Parry, D.A., Wall, J.S., Hainfeld, J.F., and Studier, F.W. (1988). Molecular substructure of a viral receptor-recognition protein. The gp17 tail-fiber of bacteriophage T7. J. Mol. Biol. *200*, 351–365.

Steven, A.C., Heymann, J.B., Cheng, N., Trus, B.L., and Conway, J.F. (2005). Virus maturation: dynamics and mechanism of a stabilizing structural transition that leads to infectivity. Curr. Opin. Struct. Biol. *15*, 227–236.

Sun, Y., Parker, M.H., Weigele, P., Casjens, S., Prevelige, P.E., Jr., and Krishna, N.R. (2000). Structure of the coat protein-binding domain of the scaffolding protein from a double-stranded DNA virus. J. Mol. Biol. *297*, 1195–1202.

Thompson, J.D., Higgins, D.G., and Gibson, T.J. (1994). CLUSTAL W: improving the sensitivity of progressive multiple sequence alignment through sequence weighting, position-specific gap penalties and weight matrix choice. Nucleic Acids Res. *22*, 4673–4680.

Tzlil, S., Kindt, J.T., Gelbart, W.M., and Ben Shaul, A. (2003). Forces and pressures in DNA packaging and release from viral capsids. Biophys. J. *84*, 1616–1627.

Valpuesta, J.M., and Carrascosa, J.L. (1994). Structure of viral connectors and their function in bacteriophage assembly and DNA packaging. Q. Rev. Biophys. *27*, 107–155.

Vriend, G. (1990). WHAT IF: a molecular modeling and drug design program. J. Mol. Graph. *8*, 52–56, 29.

Wikoff, W.R., Liljas, L., Duda, R.L., Tsuruta, H., Hendrix, R.W., and Johnson, J.E. (2000). Topologically linked protein rings in the bacteriophage HK97 capsid. Science *289*, 2129–2133.

Wriggers, W., and Birmanns, S. (2001). Using situs for flexible and rigid-body fitting of multiresolution single-molecule data. J. Struct. Biol. *133*, 193–202.

Zhou, Z.H., Baker, M.L., Jiang, W., Dougherty, M., Jakana, J., Dong, G., Lu, G., and Chiu, W. (2001). Electron cryomicroscopy and bioinformatics suggest protein fold models for rice dwarf virus. Nat. Struct. Biol. *8*, 868–873.

Accession Numbers

The T7 procapsid volume has been deposited in the 3D-EM database with accession code EMD-1321.

